

# Generalized field mixing for endpoint criticality with marginal flow: resolving the four-state Potts endpoint in the square-lattice $J_1$ - $J_2$ Ising model

Yihua Sun<sup>1,2</sup> and Yuchen Fan<sup>1,2,\*</sup>

<sup>1</sup>*Research Center for Quantum Physics and Technologies,  
Inner Mongolia University, Hohhot 010021, China*

<sup>2</sup>*School of Physical Science and Technology, Inner Mongolia University, Hohhot 010021, China*

Identifying the asymptotic criticality of a critical endpoint is challenging, as pseudo-first-order signatures persist over accessible system sizes and mask its underlying critical nature. This ambiguity is amplified at endpoints controlled by a marginally irrelevant scaling field, where logarithmic flow delays the onset of asymptotic scaling. Here we develop a generalized field-mixing framework for endpoint criticality governed by one relevant scaling field together with a marginally irrelevant one, a setting that lies outside the conventional two-relevant-field formulation. By constructing a finite-size pseudocritical manifold, the framework removes the normal relevant detuning and exposes the residual marginal drift, enabling controlled histogram- and Binder-based finite-size analyses. We apply this approach to the frustrated square-lattice  $J_1$ - $J_2$  Ising model, where the location and even the nature of the stripe-ordering endpoint have remained controversial for decades. The endpoint is isolated directly as a distinct singular point, rather than inferred from where the phase boundary appears most Potts-like, and its asymptotic criticality is shown to follow four-state Potts universality with logarithmic corrections. This identification is independently supported by direct comparison with the Potts point of the Ashkin–Teller model and by consistent Binder scaling in both the magnetic and nematic sectors. Our results resolve a longstanding numerical ambiguity in a paradigmatic frustrated Ising system and establish a general framework for extracting asymptotic endpoint criticality in the presence of marginal flow.

## I. INTRODUCTION

Determining the asymptotic nature of a phase transition from finite-size data is a central challenge in numerical studies of critical phenomena. Critical endpoints, where a continuous transition line terminates and gives way to first-order behavior, provide an especially sharp setting for this problem, as finite-size observables can display persistent first-order-like signatures even when the transition is continuous. This ambiguity is amplified by marginally irrelevant operators, whose logarithmically slow flow can obscure the asymptotic scaling over broad finite-size windows [1].

A paradigmatic example is the frustrated square-lattice  $J_1$ - $J_2$  Ising model with antiferromagnetic nearest- and next-nearest-neighbor couplings  $J_1$  and  $J_2$ , whose stripe-ordering transition has long served as a benchmark problem for endpoint criticality [2–35]. As a function of the frustration ratio  $g \equiv J_2/J_1$ , the standard scenario is a weakly first-order phase boundary for  $1/2 < g < g_{\text{ep}}$ , followed for  $g > g_{\text{ep}}$  by a line of continuous Ashkin–Teller transitions [10, 19–22]. At the endpoint  $g_{\text{ep}}$ , the transition is expected to coincide with the four-state Potts point, where a marginally irrelevant field generates logarithmically slow flow [36–38] and further complicates the distinction between the weakly first-order regime below the endpoint and the pseudo-first-order finite-size behavior above it [20, 21]. This difficulty is reflected in the long spread of numerical conclusions: early analytical [10–13]

and Monte Carlo studies [16, 19] placed the endpoint as far out as  $g_{\text{ep}} \sim 1.0$ , later Monte Carlo works established a close correspondence with the Ashkin–Teller model and suggested  $g_{\text{ep}} \approx 0.67$  [20, 21], whereas more recent infinite-size tensor-network studies have proposed scenarios ranging from  $g_{\text{ep}} \rightarrow \infty$  [29] to tricritical Ising criticality [27]. These persistent discrepancies point to the need for a numerical framework tailored to endpoint criticality.

Field mixing provides a natural language for such problems because it reorganizes the vicinity of a critical endpoint in terms of scaling directions rather than bare microscopic couplings [39–45]. In its conventional form, however, field mixing is formulated for multicritical settings governed by two relevant fields, as in the Blume–Capel model [43, 44], where it enables symmetric mixed-histogram constructions, precise localization of the tricritical point, and controlled extraction of exponents. Endpoint criticality with a marginally irrelevant field lies outside this standard setting: the tangent sector is not a second relevant direction with power-law scaling, and this marginal flow generates multiplicative logarithmic corrections to the relevant scaling variable [1]. It is therefore not evident that the conventional two-relevant-field construction remains controlled, nor how finite-size endpoint diagnostics should be reorganized in the presence of such relevant–marginal scaling structure. This leaves a methodological gap in the field-mixing framework for endpoint criticality.

Here we develop a generalized field-mixing framework for endpoint criticality governed by one relevant scaling field together with a marginally irrelevant one, and apply it to the  $J_1$ - $J_2$  endpoint as a complete two-field endpoint-

---

\* yuchenfan@imu.edu.cn

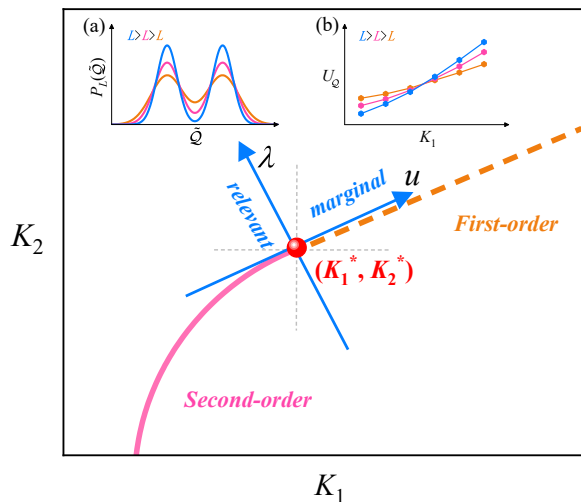


Fig. 1. Generalized field mixing for endpoint criticality with marginal flow. Schematic illustration of the generalized field-mixing framework near a critical endpoint in the  $(K_1, K_2)$  phase diagram, where a first-order line terminates on a continuous transition line. Taking the endpoint as the origin, two mixed variables are introduced:  $\lambda$  for the relevant detuning direction and  $u$  for the tangent marginally irrelevant direction. This separation enables the independent analysis of the relevant critical singularity and the residual marginal drift. Inset (a), finite-size pseudotransition points near the endpoint are determined by requiring a symmetric histogram of the centered mixed variable  $\tilde{Q}$ . Inset (b), Binder analysis performed along the finite-size pseudotransition manifold locates the endpoint through the crossing points.

scaling problem. The key step is to construct a finite-size pseudocritical manifold that removes the normal relevant detuning and exposes the residual marginal drift for direct analysis. The framework isolates the endpoint as a distinct singular point, rather than inferring it indirectly by imposing an assumed asymptotic critical behavior along the phase boundary. For the  $J_1$ - $J_2$  endpoint, this endpoint-first construction yields direct histogram-level evidence for four-state Potts universality with logarithmic corrections. This scaling structure is independently corroborated by comparison with the Potts point of the Ashkin–Teller model and by Binder analyses in both the magnetic and nematic sectors. Our results resolve a longstanding ambiguity in the  $J_1$ - $J_2$  Ising model and establish a general framework for extracting asymptotic endpoint criticality in the presence of marginal flow.

## II. GENERALIZED FIELD MIXING

We begin from the standard field-mixing construction for a Hamiltonian containing two energy-like sectors,

$$H = J_1 E_1 + J_2 E_2, \quad (1)$$

where the natural bare control parameters are the dimensionless couplings  $K_1 = \beta J_1$  and  $K_2 = \beta J_2$ , with

$\beta = 1/T$  the inverse temperature (setting  $k_B = 1$ ). The corresponding intensive energy-like operators are  $\mathcal{E}_1 \equiv L^{-d} E_1$  and  $\mathcal{E}_2 \equiv L^{-d} E_2$ . Near an endpoint  $(K_1^*, K_2^*)$ , the bare deviations  $\delta K_1 = K_1 - K_1^*$  and  $\delta K_2 = K_2 - K_2^*$  are reorganized along the local scaling directions as

$$\lambda = \delta K_2 + r \delta K_1, \quad u = \delta K_1 + s \delta K_2, \quad (2)$$

as illustrated in Fig. 1, with  $r$  and  $s$  denoting the corresponding mixing coefficients. Here  $\lambda$  parametrizes the generic normal detuning direction away from the phase boundary and therefore represents the relevant scaling field, whereas  $u$  runs locally tangent to the phase boundary and, at the endpoint, corresponds to the marginally irrelevant direction. The associated scaling operators are

$$\mathcal{Q} = \frac{1}{1-rs} (\mathcal{E}_2 - s \mathcal{E}_1), \quad \mathcal{E} = \frac{1}{1-rs} (\mathcal{E}_1 - r \mathcal{E}_2), \quad (3)$$

satisfying  $\langle \mathcal{Q} \rangle = -L^{-d} \partial_\lambda \ln Z$  and  $\langle \mathcal{E} \rangle = -L^{-d} \partial_u \ln Z$ .

Conventional field mixing assumes two relevant directions [43, 44]. Endpoint criticality with a marginally irrelevant flow is qualitatively different and therefore requires a modified finite-size scaling description. At the endpoint, the mixed scaling fields are tuned to  $\lambda = 0$  and  $u = 0$ , so the joint histogram is controlled by the scaling operators together with the logarithmic renormalization induced by the marginally irrelevant scaling field. Its joint distribution is therefore expected to obey the scaling form

$$P_L \propto \mathcal{P}^* \left( L^{d-y_t} (\ln L)^{-q} \tilde{Q}, X_u(\mathcal{E}; L) \right), \quad (4)$$

where  $\mathcal{P}^*$  is a universal scaling function,  $y_t$  is the RG eigenvalue of the relevant direction, and  $q$  denotes the corresponding logarithmic correction exponent. Here  $\tilde{Q} \equiv \mathcal{Q} - \langle \mathcal{Q} \rangle$  denotes the centered fluctuation of the scaling operator  $\mathcal{Q}$  conjugate to the relevant field  $\lambda$ . Its critical scale at the endpoint is  $L^{y_t-d} (\ln L)^q$ , making the first argument the dimensionless scaling variable for the relevant direction, while  $X_u(\mathcal{E}; L)$  represents the residual tangent variable associated with the marginally irrelevant sector. Projecting the joint distribution onto  $\tilde{Q}$ , that is, integrating out the remaining scaling direction, then gives the scaling form

$$P_L(\tilde{Q}) = L^{d-y_t} (\ln L)^{-q} \mathcal{P}_Q^* \left[ L^{d-y_t} (\ln L)^{-q} \tilde{Q} \right], \quad (5)$$

where  $\mathcal{P}_Q^*$  is the associated universal scaling function, and the prefactor  $L^{d-y_t} (\ln L)^{-q}$  is fixed by the normalization of the probability density under the finite-size scaling of  $\tilde{Q}$ .

To locate the endpoint, we analyze the histogram of  $\tilde{Q}$ , which provides a direct probe of coexistence-like finite-size behavior. For each system size, we implement this construction by fixing one bare parameter (e.g.,  $K_1$ ) and tuning the other control parameter together with the mixing coefficient  $s$  so that  $P_L(\tilde{Q})$  is maximally symmetric (as schematically illustrated in inset a of Fig. 1). On

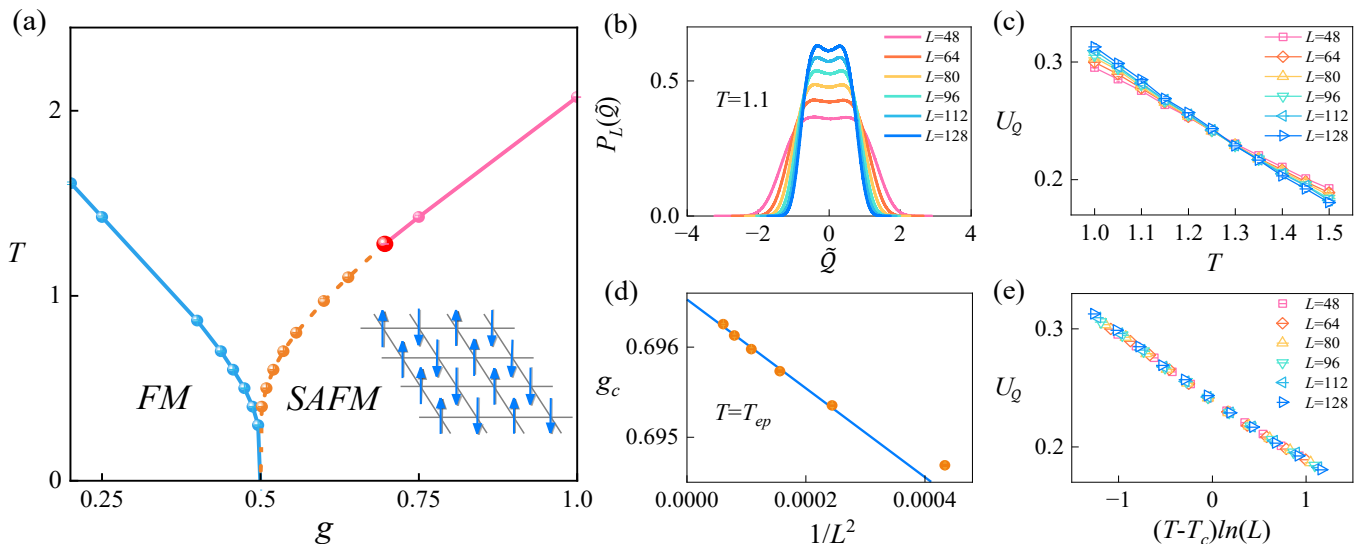


Fig. 2. Location of the endpoint in the square-lattice  $J_1$ - $J_2$  Ising model. (a) Phase diagram of the square-lattice  $J_1$ - $J_2$  Ising model. The transition from the SAFM phase to the paramagnetic phase is first order at low temperatures and continuous at higher temperatures, with the endpoint located at  $(g_{\text{ep}}, T_{\text{ep}}) = (0.696(10), 1.28(3))$ . (b) Maximally symmetric histograms  $P_L(\tilde{Q})$  at  $T = 1.1$  for different system sizes. The symmetry condition determines the finite-size pseudotransition point, at which the fourth-order cumulant  $U_{\tilde{Q}}$  is evaluated. (c) Fourth-order cumulant  $U_{\tilde{Q}}$  measured along the finite-size pseudotransition manifold. The crossings for different system sizes provide an estimate of the endpoint temperature  $T_{\text{ep}} = 1.28(3)$ . (d) Finite-size pseudotransition couplings  $g_c(L)$  at  $T = T_{\text{ep}} = 1.28$ , extracted from the maximally symmetric endpoint histograms shown in Fig. 3(a). Extrapolating  $g_c(L)$  to the thermodynamic limit gives the conditional estimate  $g_{\text{ep}}|_{T=1.28} = 0.6965(3)$ . (e) Finite-size scaling analysis of  $U_{\tilde{Q}}$  near the endpoint with logarithmic finite-size dependence.

the first-order side, this reduces to the usual equal-weight condition; beyond the endpoint, it extends smoothly into the pseudo-first-order regime. The symmetric-histogram points thus define the finite-size pseudotransition manifold along which the normal relevant detuning is tuned to zero. Along this manifold, we evaluate the fourth-order cumulant

$$U_{\tilde{Q}}(L) = 1 - \frac{\langle \tilde{Q}^4 \rangle}{3\langle \tilde{Q}^2 \rangle^2}, \quad (6)$$

and use its finite-size crossings to locate the endpoint (as schematically illustrated in inset b of Fig. 1). Once the relevant detuning has been eliminated in this way, the leading size dependence of  $U_{\tilde{Q}}$  is governed by the marginally irrelevant sector.

### III. RESULTS

#### A. The square-lattice $J_1$ - $J_2$ Ising model and endpoint identification

We now apply the generalized field-mixing framework to the frustrated square-lattice  $J_1$ - $J_2$  Ising model, with Hamiltonian

$$H = J_1 \sum_{\langle ij \rangle} \sigma_i \sigma_j + J_2 \sum_{\langle\langle ij \rangle\rangle} \sigma_i \sigma_j, \quad (7)$$

where  $\sigma_i = \pm 1$  are Ising spins. We take  $J_1 < 0$  and  $J_2 > 0$ , corresponding to ferromagnetic nearest-neighbor and antiferromagnetic next-nearest-neighbor couplings. This convention is equivalent, under a staggered gauge transformation, to the choice  $J_1 > 0$ ,  $J_2 > 0$ . Throughout this work we set  $|J_1| = 1$  and parametrize frustration by  $g \equiv J_2/|J_1|$ .

At zero temperature, the model has two ordered phases: a ferromagnetic (FM) phase at small  $g$  and a stripe antiferromagnetic (SAFM) phase for  $g > 1/2$ . Because the SAFM state breaks the lattice  $Z_4$  symmetry, the continuous part of its thermal phase boundary is expected to belong to the Ashkin-Teller (AT) universality class, terminating at a four-state Potts endpoint that separates the low-temperature first-order segment from the high-temperature continuous branch [20, 21]. This is precisely the setting in which endpoint criticality is governed by one relevant field together with a marginally irrelevant one [36–38]. At the same time, the location and even the nature of this endpoint remain highly controversial: even within the four-state Potts scenario, proposed positions range from  $g_{\text{ep}} \approx 0.67$  [20, 21] to the limiting case  $g_{\text{ep}} \rightarrow \infty$  [29], whereas one recent study instead identifies the endpoint as tricritical Ising [27]. This persistent ambiguity reflects the logarithmically slow marginal flow expected in the four-state Potts scenario and the accompanying pseudo-first-order behavior that can remain prominent over broad finite-size windows, thereby obscuring the asymptotic endpoint scaling.

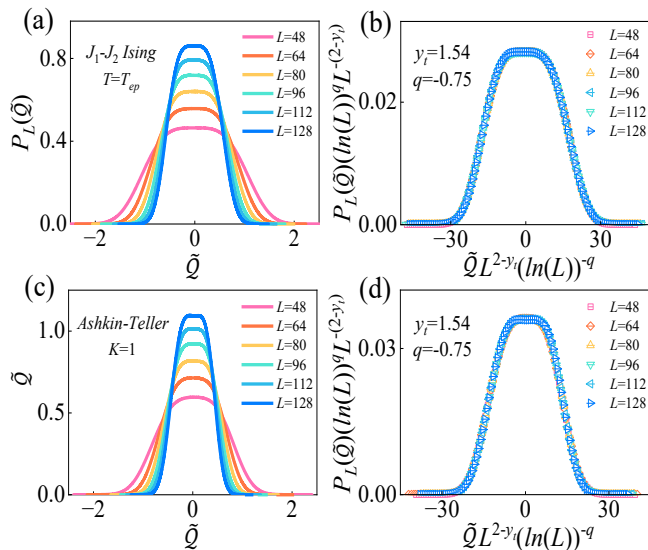


Fig. 3. Histogram scaling at the endpoint and comparison with the Ashkin–Teller Potts point. (a) Maximally symmetric histograms  $P_L(\tilde{Q})$  at  $T = T_{ep}$  of the square-lattice  $J_1$ – $J_2$  Ising model for different system sizes. (b) Finite-size scaling collapse of the endpoint histograms shown in (a), using the logarithmically corrected four-state Potts histogram scaling form. (c) Maximally symmetric histograms  $P_L(\tilde{Q})$  at the four-state Potts point of the Ashkin–Teller model for different system sizes. (d) Logarithmically corrected finite-size scaling collapse of the histograms in (c).

We perform large-scale Monte Carlo simulations on square lattices of size  $L \times L$  with periodic boundary conditions, using system sizes up to  $L = 128$ . For histogram-based measurements, we employ a single long Markov chain and accumulate at least  $10^7$  samples after thermalization, while for parameter points in the immediate vicinity of the endpoint the statistics are further increased to  $10^8$ . Convergence is checked by confirming that both the histograms and the fourth-order cumulant  $U_Q$  remain stable upon further increasing the sampling statistics. For standard observables, we run multiple independent Markov chains in parallel (typically 56–112) to improve statistics. For each parameter set, each chain is equilibrated for at least  $10^6$  Monte Carlo sweeps (MCS) and then continued for at least  $10^6$  MCS for measurements.

We now turn to the direct numerical identification of the endpoint, the first step of the generalized field-mixing analysis, as summarized in Fig. 2. Fig. 2(a) shows that the SAFM–paramagnetic transition is first order at low temperatures and continuous at higher temperatures, with the two branches meeting at  $(g_{ep}, T_{ep}) = (0.696(10), 1.28(3))$ . Representative transition-point determinations away from the endpoint are shown in Figs. S1 and S2. As illustrated in Fig. 2(b), for each system size we construct the finite-size pseudotransition point at a fixed temperature by tuning  $g$  and  $s$  to impose maximal symmetry on the histogram of the centered

mixed variable  $\tilde{Q}$ . This criterion extends smoothly into the pseudo-first-order regime and yields both the finite-size pseudotransition point and the corresponding fourth-order cumulant  $U_Q$ . Evaluating  $U_Q$  along this manifold [Fig. 2(c)] gives the endpoint temperature  $T_{ep}$  from the crossings, while extrapolation of the associated finite-size pseudotransition couplings  $g_c(L)$  at  $T = T_{ep}$  [Fig. 2(d)] yields the thermodynamic-limit endpoint coupling  $g_{ep}$ . Fig. 2(e) provides the corresponding scaling test: once the normal relevant detuning is removed, the residual drift of  $U_Q$  is not organized by the power-law behavior expected for a second relevant field, but instead follows an approximately logarithmic dependence.

## B. Histogram scaling at the endpoint

We next examine the endpoint histogram and its finite-size scaling. Figure 3(a) shows the maximally symmetric histograms  $P_L(\tilde{Q})$  at the endpoint temperature  $T = T_{ep}$ . At accessible system sizes, these endpoint histograms still display a weakly developed, nearly flat two-peak profile, superficially similar to the coexistence histograms found along the first-order line. Since the first-order line terminates at the endpoint, these first-order-like features should be understood as finite-size pseudo-first-order effects rather than evidence of phase coexistence. This interpretation is supported by earlier work on the same model, where pseudo-first-order behavior and the limited diagnostic value of first-order-like histogram features were explicitly discussed [20–22, 46]. Related pseudo-first-order signatures have likewise been reported in the Baxter–Wu model, another system in the four-state Potts universality class [47].

Within the generalized field-mixing framework, the endpoint histogram can be analyzed directly through controlled finite-size scaling. For the four-state Potts endpoint, a marginally irrelevant operator generates multiplicative logarithmic corrections [36–38]. As a result, the relevant thermal scaling field enters the finite-size scaling variable in the form  $\lambda(L) \sim \lambda L^{y_t}(\ln L)^q$ , with  $y_t = 3/2$  and  $q = -3/4$  [37]. The fluctuation scale of the conjugate scaling operator is therefore expected to behave as  $\tilde{Q} \sim L^{y_t-d}(\ln L)^q$ , thereby fixing the scaling exponents entering Eq. (5). As illustrated in Fig. 3(b), the endpoint histograms collapse according to the logarithmically corrected four-state Potts scaling form, providing a direct histogram-level test of the endpoint scaling.

To make this identification concrete, we benchmark the  $J_1$ – $J_2$  endpoint against the Ashkin–Teller (AT) model at the Potts point (for background on the AT model, see Refs. [48–50]). We consider the standard Hamiltonian

$$H_{AT} = -J \sum_{\langle ij \rangle} (\sigma_i \sigma_j + \tau_i \tau_j) - K \sum_{\langle ij \rangle} \sigma_i \sigma_j \tau_i \tau_j, \quad (8)$$

where  $\sigma_i, \tau_i = \pm 1$  are two Ising variables on each site, and we set  $J = 1$  for simplicity. In the field-mixing description, this model naturally contains the

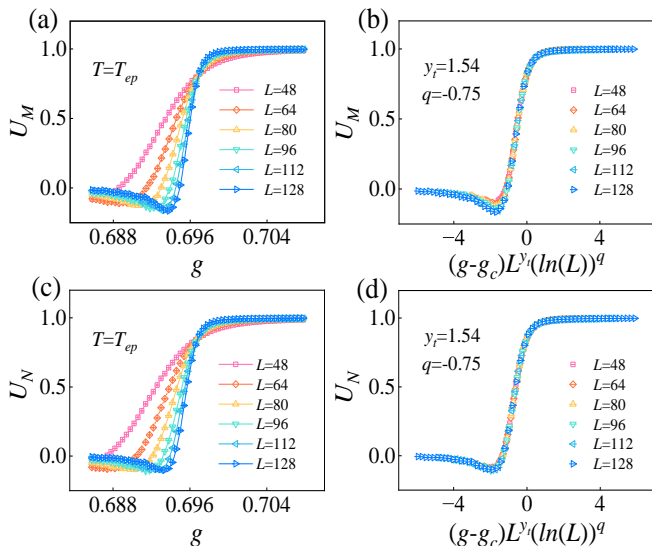


Fig. 4. Logarithmically corrected Binder scaling in the magnetic and nematic sectors. (a) Binder cumulant of the stripe magnetic order parameter at  $T = T_{\text{ep}}$  as a function of  $g$  for different system sizes, with crossings at the endpoint coupling  $g_c = 0.6968(2)$ . (b) Finite-size scaling collapse of the magnetic Binder data using the logarithmically corrected four-state Potts scaling form. (c) Binder cumulant of the nematic order parameter at the same temperature, with crossings at the same endpoint coupling. (d) Finite-size scaling collapse of the nematic Binder data using the same scaling form.

same two energy-like sectors: the quadratic spin interaction  $E_1 = \sum_{\langle ij \rangle} (\sigma_i \sigma_j + \tau_i \tau_j)$  and the four-spin interaction  $E_2 = \sum_{\langle ij \rangle} \sigma_i \sigma_j \tau_i \tau_j$ , whose mixed combination defines the scaling operator  $\mathcal{Q}$ . At the Potts point  $K = 1$  on the critical line, the histograms of  $\hat{\mathcal{Q}}$  [Fig. 3(c)] exhibit finite-size structures similar to those of the  $J_1$ - $J_2$  endpoint, and the same logarithmically corrected collapse is obtained in Fig. 3(d). This benchmark validates the generalized field-mixing construction in a known relevant-marginal Potts setting and supports the identification of the  $J_1$ - $J_2$  endpoint with four-state Potts criticality.

### C. Independent confirmation from Binder scaling

With the endpoint identified by the field-mixing construction, we further test its critical structure through dimensionless Binder cumulants defined in complementary sectors of the stripe order. Using the standard definitions of Refs. [20, 21], we first consider the two-component magnetic order parameter  $\mathbf{m} = (m_x, m_y)$ , with  $m_x = \frac{1}{L^2} \sum_i \sigma_i (-1)^{x_i}$ ,  $m_y = \frac{1}{L^2} \sum_i \sigma_i (-1)^{y_i}$ , where  $L^2$  is the number of sites,  $(x_i, y_i)$  are the integer lattice coordinates of site  $i$ , and  $m^2 = m_x^2 + m_y^2$ . The associated Binder cumulant

$$U_M = 2 \left( 1 - \frac{1}{2} \frac{\langle m^4 \rangle}{\langle m^2 \rangle^2} \right) \quad (9)$$

probes the magnetic sector of the stripe order. To resolve the orientational component of the same  $Z_4$  stripe order, we further introduce the bond-nematic order parameter  $N = \frac{1}{L^2} \sum_i (\sigma_i \sigma_{i+\hat{x}} - \sigma_i \sigma_{i+\hat{y}})$ , where  $\hat{x}$  and  $\hat{y}$  denote the nearest-neighbor unit vectors along the two lattice directions. Its Binder cumulant is defined as

$$U_N = \frac{3}{2} \left( 1 - \frac{\langle N^4 \rangle}{3 \langle N^2 \rangle^2} \right). \quad (10)$$

Near the endpoint, we analyze Binder cumulants along the fixed- $T$  cut  $T = T_{\text{ep}}$ . Since this cut generically projects onto the relevant scaling direction, their finite-size scaling takes the form [37],

$$U(g, L) = \mathcal{U}[(g - g_{\text{ep}})L^{y_t}(\ln L)^q], \quad (11)$$

with  $\mathcal{U}$  a universal scaling function. Figure 4(a) shows the magnetic Binder cumulant  $U_M$  versus  $g$  for different system sizes, with crossings converging to  $g_c = 0.6968(2)$ , in agreement with the endpoint position inferred from Fig. 2(d). Although a negative Binder dip is commonly associated with phase coexistence and first-order behavior [51, 52], the pronounced dip in  $U_M$  here reflects pseudo-first-order finite-size behavior near the Potts endpoint rather than a true first-order transition. The coexistence-like signatures underlying the negative Binder dip can be visualized directly in the corresponding  $\mathbf{m}$  and  $m^2$  histograms (see Fig. S3). Including the logarithmic correction required by the four-state Potts RG structure allows the magnetic Binder data to collapse onto a single scaling curve [Fig. 4(b)]. Figures 4(c) and 4(d) show that the nematic Binder cumulant  $U_N$  exhibits the same crossing point and the same logarithmically corrected scaling behavior, confirming that the identified Potts endpoint criticality is robust across complementary sectors of the underlying  $Z_4$  stripe order.

## IV. DISCUSSION

The central advance of our work is to recast the long-standing Potts-endpoint controversy in the  $J_1$ - $J_2$  Ising model as a two-field endpoint-scaling problem. This shift is essential because the ambiguity surrounding the stripe-ordering endpoint is not merely a matter of numerical resolution, but reflects the relevant-marginal structure of the endpoint itself. Near the endpoint, the logarithmically slow flow of the marginally irrelevant field gives rise to broad finite-size regimes in which pronounced pseudo-first-order signatures coexist with the underlying asymptotic Potts criticality. The generalized field-mixing construction developed here separates the normal relevant detuning from the tangent marginal drift and resolves this finite-size diagnostic problem by explicitly accounting for the full relevant-marginal scaling structure of the endpoint.

This endpoint-scaling perspective also clarifies how our results build on and extend earlier studies [20, 21],

which established the importance of pseudo-first-order behavior and gave strong evidence that the continuous branch terminates at a four-state Potts point. However, because the endpoint was inferred mainly from behavior along the phase boundary, the finite-size ambiguity left room for competing interpretations. One distinguishing feature of the present analysis is its endpoint-first character: the endpoint is isolated by combining a mixed-histogram construction with Binder crossings along the finite-size pseudotransition manifold, rather than inferred indirectly from apparent Potts-like behavior along the phase boundary. In this construction, the first-order-like histogram structure is not merely an ambiguity to be avoided; its symmetry is the defining criterion for that manifold. Moreover, the mixed histogram is not used merely as a qualitative indicator of coexistence-like finite-size behavior, but as a direct scaling test of the logarithmically corrected Potts scaling form. In this way, our work does not simply reaffirm the Potts scenario, but

resolves the remaining ambiguity through a comprehensive endpoint-scaling analysis.

More broadly, the present work closes a methodological gap in the standard field-mixing framework by extending it beyond its conventional two-relevant-field formulation [43, 44] to endpoint criticality governed by one relevant field and one marginally irrelevant field. The generalized field mixing developed here therefore provides a route to resolving endpoint criticality in relevant–marginal settings. Its underlying principle—disentangling multiple scaling directions—may shed light on more complex multicritical and endpoint problems.

### Acknowledgements

We thank Rong Yu, Changle Liu, and Yuan Wan for valuable help. The authors acknowledge supports by the National Natural Science Foundation of China (Grants No. 12404176 and No. 12564022).

- 
- [1] John Cardy, “Scaling and Renormalization in Statistical Physics,” (Cambridge University Press, 1996).
- [2] M.P. Nightingale, “Non-universality for ising-like spin systems,” *Physics Letters A* **59**, 486–488 (1977).
- [3] M N Barber, “Non-universality in the ising model with nearest and next-nearest neighbour interactions,” *Journal of Physics A: Mathematical and General* **12**, 679 (1979).
- [4] Robert H. Swendsen and Samuel Krinsky, “Monte carlo renormalization group and ising models with  $n \geq 2$ ,” *Phys. Rev. Lett.* **43**, 177–180 (1979).
- [5] J Oitmaa, “The square-lattice ising model with first and second neighbour interactions,” *Journal of Physics A: Mathematical and General* **14**, 1159 (1981).
- [6] K. Binder and D. P. Landau, “Phase diagrams and critical behavior in ising square lattices with nearest- and next-nearest-neighbor interactions,” *Phys. Rev. B* **21**, 1941–1962 (1980).
- [7] D. P. Landau, “Phase transitions in the ising square lattice with next-nearest-neighbor interactions,” *Phys. Rev. B* **21**, 1285–1297 (1980).
- [8] D. P. Landau and K. Binder, “Phase diagrams and critical behavior of ising square lattices with nearest-, next-nearest-, and third-nearest-neighbor couplings,” *Phys. Rev. B* **31**, 5946–5953 (1985).
- [9] F Aguilera-Granja and J L Moran-Lopez, “Specific heat and the phase diagram of the ising square lattice with nearest- and next-nearest interactions,” *Journal of Physics: Condensed Matter* **5**, A195 (1993).
- [10] J. L. Morán-López, F. Aguilera-Granja, and J. M. Sanchez, “First-order phase transitions in the ising square lattice with first- and second-neighbor interactions,” *Phys. Rev. B* **48**, 3519–3522 (1993).
- [11] J L Moran-Lopez, F Aguilera-Granja, and J M Sanchez, “Phase transitions in ising square antiferromagnets with first- and second-neighbour interactions,” *Journal of Physics: Condensed Matter* **6**, 9759 (1994).
- [12] E. López-Sandoval, J.L. Morán-López, and F. Aguilera-Granja, “Cluster variation method and monte carlo simulations in ising square antiferromagnets,” *Solid State Communications* **112**, 437–441 (1999).
- [13] Rosana A. dos Anjos, J. Roberto Viana, and J. Ricardo de Sousa, “Phase diagram of the ising antiferromagnet with nearest-neighbor and next-nearest-neighbor interactions on a square lattice,” *Physics Letters A* **372**, 1180–1184 (2008).
- [14] James L. Monroe and Seung-Yeon Kim, “Phase diagram and critical exponent  $\nu$  for the nearest-neighbor and next-nearest-neighbor interaction ising model,” *Phys. Rev. E* **76**, 021123 (2007).
- [15] A. Malakis, P. Kalozoumis, and N. Tyraskis, “Monte carlo studies of the square ising model with next-nearest-neighbor interactions,” *The European Physical Journal B - Condensed Matter and Complex Systems* **50**, 63–67 (2006).
- [16] A. Kalz, A. Honecker, S. Fuchs, and T. Pruschke, “Phase diagram of the ising square lattice with competing interactions,” *The European Physical Journal B* **65**, 533 (2008).
- [17] A Kalz, A Honecker, S Fuchs, and T Pruschke, “Monte carlo studies of the ising square lattice with competing interactions,” *Journal of Physics: Conference Series* **145**, 012051 (2009).
- [18] A. K. Murtazaev, M. K. Ramazanov, and M. K. Badiev, “Critical properties of an antiferromagnetic ising model on a square lattice with interactions of the next-to-nearest neighbors,” *Low Temperature Physics* **37**, 1001–1005 (2011).
- [19] Ansgar Kalz, Andreas Honecker, and Marion Moliner, “Analysis of the phase transition for the ising model on the frustrated square lattice,” *Phys. Rev. B* **84**, 174407 (2011).
- [20] Songbo Jin, Arnab Sen, and Anders W. Sandvik, “Ashkin-teller criticality and pseudo-first-order behavior in a frustrated ising model on the square lattice,” *Phys. Rev. Lett.* **108**, 045702 (2012).
- [21] Songbo Jin, Arnab Sen, Wenan Guo, and Anders W. Sandvik, “Phase transitions in the frustrated ising model

- on the square lattice,” *Phys. Rev. B* **87**, 144406 (2013).
- [22] Ansgar Kalz and Andreas Honecker, “Location of the potts-critical end point in the frustrated ising model on the square lattice,” *Phys. Rev. B* **86**, 134410 (2012).
- [23] A. K. Murtazaev, M. K. Ramazanov, F. A. Kassan-Ogly, and M. K. Badiev, “Phase transitions in the antiferromagnetic ising model on a square lattice with next-nearest-neighbor interactions,” *Journal of Experimental and Theoretical Physics* **117**, 1091–1096 (2013).
- [24] A. Bobák, T. Lučivjanský, M. Borovský, and M. Žukovič, “Phase transitions in a frustrated ising antiferromagnet on a square lattice,” *Phys. Rev. E* **91**, 032145 (2015).
- [25] A.K. Murtazaev, M.K. Ramazanov, and M.K. Badiev, “Critical properties of the two-dimensional ising model on a square lattice with competing interactions,” *Physica B: Condensed Matter* **476**, 1–5 (2015).
- [26] M.K. Ramazanov, A.K. Murtazaev, and M.A. Magomedov, “Thermodynamic, critical properties and phase transitions of the ising model on a square lattice with competing interactions,” *Solid State Communications* **233**, 35–40 (2016).
- [27] Hong Li and Li-Ping Yang, “Tensor network simulation for the frustrated  $J_1$ – $J_2$  ising model on the square lattice,” *Phys. Rev. E* **104**, 024118 (2021).
- [28] Kota Yoshiyama and Koji Hukushima, “Higher-order tensor renormalization group study of the  $J_1$ – $J_2$  ising model on a square lattice,” *Phys. Rev. E* **108**, 054124 (2023).
- [29] Adil A. Gangat, “Weak first-order phase transitions in the frustrated square lattice  $J_1$ – $J_2$  classical ising model,” *Phys. Rev. B* **109**, 104419 (2024).
- [30] Christophe Chatelain, “First-order transition and marginal critical behavior in a two-dimensional frustrated ising model with efficient tensor-network implementation,” *Phys. Rev. E* **111**, 024109 (2025).
- [31] Yi Hu and Patrick Charbonneau, “Numerical transfer matrix study of frustrated next-nearest-neighbor ising models on square lattices,” *Phys. Rev. B* **104**, 144429 (2021).
- [32] V. A. Abalmasov and B. E. Vugmeister, “Metastable states in the  $J_1$ – $J_2$  ising model,” *Phys. Rev. E* **107**, 034124 (2023).
- [33] Jae Hwan Lee, Seung-Yeon Kim, and Jin Min Kim, “Frustrated ising model with competing interactions on a square lattice,” *Phys. Rev. B* **109**, 064422 (2024).
- [34] Shang-Wei Li and Fu-Jiun Jiang, “A comprehensive study of the phase transitions of the frustrated  $j_1$ - $j_2$  ising model on the square lattice,” *Progress of Theoretical and Experimental Physics* **2024**, 053A06 (2024).
- [35] Burak Çivitcioglu, Rudolf A. Römer, and Andreas Honecker, “Phase determination with and without deep learning,” *Phys. Rev. E* **111**, 024131 (2025).
- [36] M. Nauenberg and D. J. Scalapino, “Singularities and scaling functions at the potts-model multicritical point,” *Phys. Rev. Lett.* **44**, 837–840 (1980).
- [37] Jesús Salas and Alan D. Sokal, “Logarithmic corrections and finite-size scaling in the two-dimensional 4-state potts model,” *J. Stat. Phys.* **88**, 567–615 (1997).
- [38] John L. Cardy, M. Nauenberg, and D. J. Scalapino, “Scaling theory of the potts-model multicritical point,” *Phys. Rev. B* **22**, 2560–2568 (1980).
- [39] A. D. Bruce and N. B. Wilding, “Scaling fields and universality of the liquid-gas critical point,” *Phys. Rev. Lett.* **68**, 193–196 (1992).
- [40] N B Wilding and A D Bruce, “Density fluctuations and field mixing in the critical fluid,” *Journal of Physics: Condensed Matter* **4**, 3087 (1992).
- [41] N. B. Wilding and P. Nielaba, “Tricritical universality in a two-dimensional spin fluid,” *Phys. Rev. E* **53**, 926–934 (1996).
- [42] J.A. Plascak and P.H.L. Martins, “Probability distribution function of the order parameter: Mixing fields and universality,” *Computer Physics Communications* **184**, 259–269 (2013).
- [43] Wooseop Kwak, Joohyeok Jeong, Juhee Lee, and Dong-Hee Kim, “First-order phase transition and tricritical scaling behavior of the blume-capel model: A wangledau sampling approach,” *Phys. Rev. E* **92**, 022134 (2015).
- [44] Dimitrios Mataragkas, Alexandros Vasilopoulos, Nikolaos G. Fytas, and Dong-Hee Kim, “Tricriticality and finite-size scaling in the triangular blume-capel ferromagnet,” *Phys. Rev. Res.* **7**, 013214 (2025).
- [45] Yuchen Fan, “Liquid-gas analog multicriticality in a frustrated ising bilayer,” *Phys. Rev. B* **112**, 155109 (2025).
- [46] Anders W. Sandvik, “Computational studies of quantum spin systems,” *AIP Conference Proceedings* **1297**, 135–338 (2010).
- [47] Nir Schreiber and Joan Adler, “Monte carlo study of the pure and dilute baxter–wu model,” *Journal of Physics A: Mathematical and General* **38**, 7253 (2005).
- [48] Rodney J. Baxter, *Exactly Solved Models in Statistical Mechanics* (Academic Press, San Diego, CA, 1982).
- [49] Bernard Nienhuis, *Phase Transitions and Critical Phenomena*, edited by Cyril Domb and Joel L. Lebowitz, Vol. 11 (Academic Press, San Diego, CA, 1987).
- [50] Gesualdo Delfino and Paolo Grinza, “Universal ratios along a line of critical points. the ashkin–teller model,” *Nuclear Physics B* **682**, 521–550 (2004).
- [51] K. Binder and D. P. Landau, “Finite-size scaling at first-order phase transitions,” *Phys. Rev. B* **30**, 1477–1485 (1984).
- [52] Katharina Vollmayr, Joseph D. Reger, Manfred Scheucher, and Kurt Binder, “Finite size effects at thermally-driven first order phase transitions: A phenomenological theory of the order parameter distribution,” *Z. Phys. B* **91**, 113–125 (1993).

## Supplementary Information for

Generalized field mixing for endpoint criticality with marginal flow: resolving the four-state Potts endpoint in the square-lattice  $J_1$ - $J_2$  Ising model

Yihua Sun and Yuchen Fan

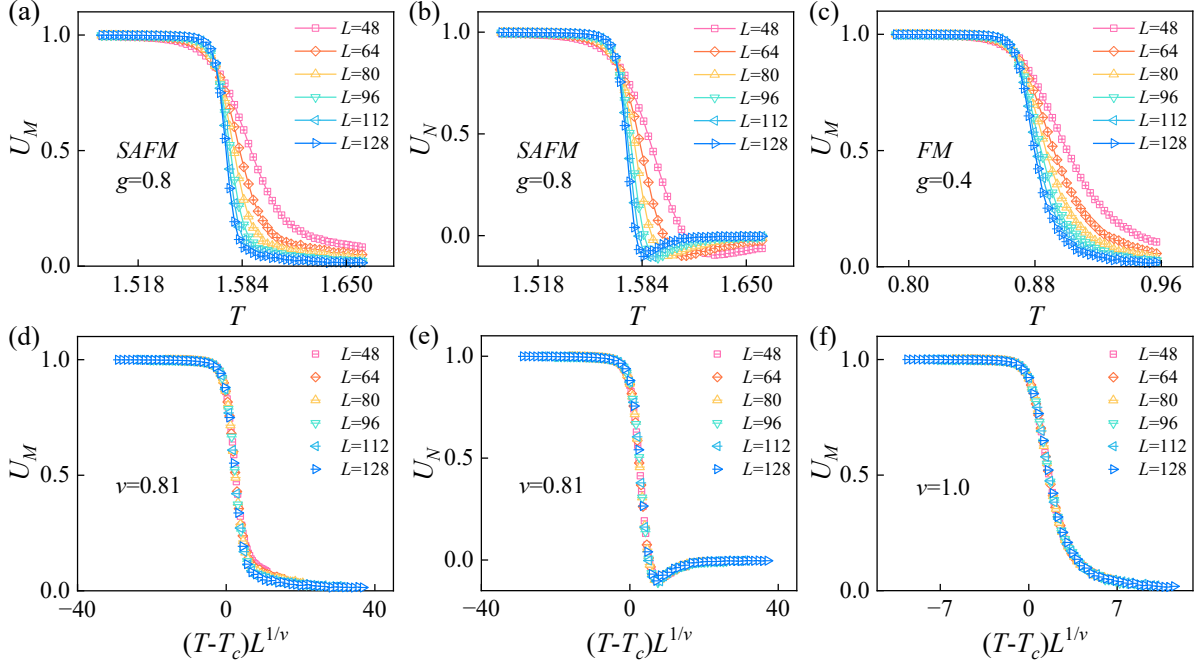


Fig. S1. Binder analysis of representative continuous transitions in the square-lattice  $J_1$ - $J_2$  Ising model. (a,b) Magnetic and nematic Binder cumulants,  $U_M$  and  $U_N$ , for the stripe-paramagnetic transition at  $g = 0.8$ . The crossings of both Binder ratios locate a common transition temperature,  $T_c = 1.5675(4)$ . (c) Binder crossing analysis for the ferromagnetic-paramagnetic transition at  $g = 0.4$ . (d,e) Finite-size scaling collapses of  $U_M$  and  $U_N$  in (a,b), giving consistent estimates of the critical exponent  $\nu$ . (f) Finite-size scaling collapse of the data in (c), showing behavior consistent with the two-dimensional Ising universality class.

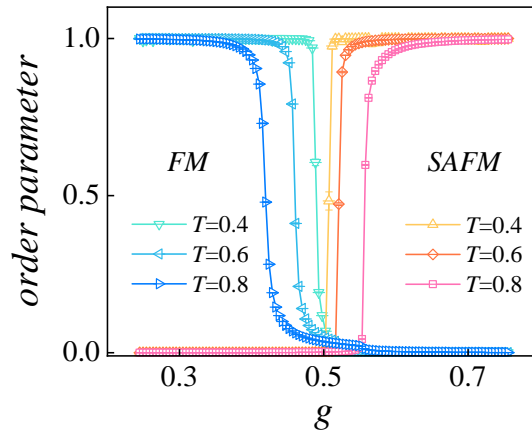


Fig. S2. Order-parameter evolution across the phase diagram at fixed temperatures. We plot the ferromagnetic order parameter  $M_{\text{FM}} = \langle |\frac{1}{L^2} \sum_i \sigma_i| \rangle$  and the stripe order parameter  $M_{\text{SAFM}} = \langle \sqrt{m_x^2 + m_y^2} \rangle$ . The disappearance of the FM order and the onset of the stripe order determine the corresponding transition points at each temperature. Upon lowering the temperature, the two transition points approach each other. Lower temperatures are not shown because equilibration becomes increasingly slow in the low-temperature first-order regime.

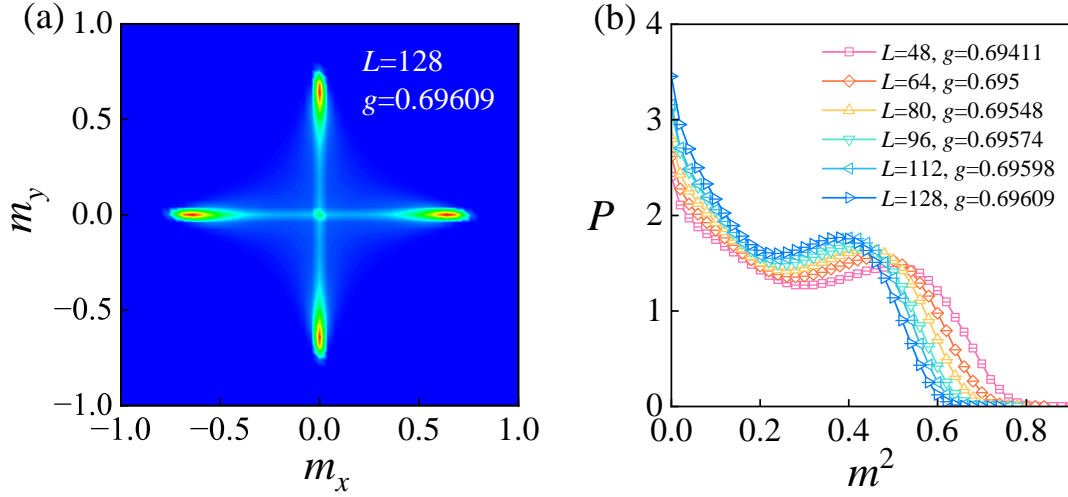


Fig. S3. Order-parameter histograms associated with the negative magnetic Binder dip at  $T = T_{\text{ep}}$ . (a) Two-dimensional histograms of the stripe magnetic order parameter  $\mathbf{m} = (m_x, m_y)$  near the Potts endpoint. (b) Corresponding probability-density histograms of  $m^2 = m_x^2 + m_y^2$ . For each system size, the coupling  $g$  is chosen by the equal-weight condition between the ordered and disordered peaks, where the distributions exhibit a pronounced bimodal structure. The coexistence-like structures visible in both representations provide a direct visualization of the finite-size origin of the negative dip in  $U_M$  shown in Fig. 4(a). As discussed in the main text, these signatures reflect pseudo-first-order finite-size behavior near the four-state Potts endpoint and should not be interpreted as evidence for a true first-order transition.